

Article

# UAV and Structure from Motion Approach to Monitor the Maierato Landslide Evolution

Danilo Godone <sup>1</sup>, Paolo Allasia <sup>1,\*</sup>, Luigi Borrelli <sup>2</sup> and Giovanni Gullà <sup>2</sup>

<sup>1</sup> Research Institute for Geo-Hydrological Protection (CNR-IRPI) Turin, National Research Council of Italy, Torino 10135, Italy; danilo.godone@irpi.cnr.it

<sup>2</sup> Research Institute for Geo-Hydrological Protection (CNR-IRPI) Rende, National Research Council of Italy, Cosenza 87036, Italy; luigi.borrelli@irpi.cnr.it (L.B.); giovanni.gulla@irpi.cnr.it (G.G.)

\* Correspondence: paolo.allasia@irpi.cnr.it

Received: 14 February 2020; Accepted: 21 March 2020; Published: 24 March 2020



**Abstract:** In February 2010 a large landslide affected the Maierato municipality (Calabria, Italy). The landslide, mainly caused by a period of prolonged and intense rainfalls, produced a mass displacement of about 5 million m<sup>3</sup> and several damages to farmlands, houses and infrastructures. In the aftermath several conventional monitoring actions were carried out. In the current post emergency phase, the monitoring was resumed by carrying out unmanned aerial vehicles (UAV) flights in order to describe the recent behavior of the landslide and to assess residual risk. Thanks to the potentialities of the structure from motion algorithms and the availability of post emergency reconnaissance photos and a previous 3D dataset, the three-dimensional evolution of the area was computed. Moreover, an experimental multispectral flight was carried out and its results supported the interpretation of local phenomena. The dataset allowed to quantify the elevation losses and raises in several peculiar sectors of the landslide. The obtained results confirm that the UAV monitoring and the structure from motion approach can effectively contribute to manage residual risk in the medium and long term within an integrated geotechnical monitoring network.

**Keywords:** GIS analysis; large landslide; monitoring; residual risk; RPAS; salvaged datasets

## 1. Introduction

Landslides are calamitous events that can heavily affect human communities and in the current global change scenario, these outcomes, in the same way as others hazards, can be even worsened [1,2]. Landslide consequences can result in several damages and, in the worst case, in casualties; moreover, the larger is the size of landslide the higher are the probabilities of occurrence of these effects [3]; equally, widespread small size landslides can have the same kind of consequences [4]. After a landslide event the activation of monitoring procedures is mandatory, in order to investigate the kinematic of the occurred phenomenon, to assess the possible triggering factors and to measure the evolution in the post emergency phase with several purposes, such as coordinating the rescue teams and evaluate the recovery actions [5–7]. In a next phase, the monitoring must be carried out to screen the residual risks potentially increased by the evolution of the landslide. The continuation of monitoring actions, from emergency phase to the ordinary one, for an adequate time span, is an efficient way to define the landslide geotechnical model in order to describe its typology and identify the best solutions to deal with residual risk like adaptation, mitigation and risk reduction [8]. Moreover, in ordinary conditions, due to their high impact on human society, landslides need to be carefully monitored in order to observe their evolution and potential threats with the aim of reducing their impact on properties and persons [9,10].

Landslide monitoring can be carried out with various techniques and approaches. They are characterized by different temporal and spatial resolutions [11–13] and their effectiveness depends on the contexts in which they are applied. Geotechnical monitoring can rely on conventional tools like extensometers, inclinometer and piezometers [10,14,15] or advanced ones like fiber optics [16] or automated inclinometers [17,18] that monitor the surficial or deep behavior of the landslide [18,19]. Geodetic techniques are based on the survey of a network of selected points in the landslide body and displacements computation; traditionally they were carried out by optical geodetic instruments. Nowadays, the employed ones are total stations (with integrated electronic distance meters) [20] or GNSS [21]. Remote techniques, based on terrestrial or air- or space-borne sensors provide an extensive survey of the investigated phenomena, usually to the detriment of temporal resolution. Sensor can be, generally subdivided in active [22,23] or passive ones [24–27].

Unmanned aerial vehicles (UAVs), among landslide monitoring techniques, are widely spreading [28]. Their versatility allows in fact the rapid execution of survey campaign and the acquisition of geocoded data. They have rapidly evolved as long as the data processing technologies; the most remarkable improvements are the development of low-cost flight control systems [29], and the diffusion of structure from motion (SfM) based software that allows the creation of a 3D model from a sequence of multi views captured images [30] and to reconstruct the morphology of the investigated area in details [31]. Several authors have proven the feasibility of UAV landslide monitoring e.g., [29,30] which provides a cheaper, and faster way for surveying of extensive surfaces [32]; which can be effectively integrated with previous conventional monitoring campaigns [33]. It also eases repeatability of the survey as UAV are easy to deploy and allow to access rugged or unsafe areas. The system is also adaptable to different kind of on-board sensors that can range from RGB cameras to multispectral ones, thermal sensors or even LiDAR [28,34].

As explained above, following a rainfall induced landslide event occurred on 15 February 2010 in the Maierato municipality (Calabria, southern Italy; Figure 1A) [35–40] survey campaigns were carried out and a preliminary monitoring network was established [7]. The landslide, that affected the left slope of the Scotrapiti Torrent (Figure 1A), destroyed a part of the S.P. 55 provincial road (about 800 m length) that allow the access to the municipality, moved a building of about 100 m and caused a loss of about 18 ha of farmland. The landslide, that involved a volume of about 5 million cubic meters, represents the reactivation of a preexisting one [35]. It is classified as a complex movement consisting of a very rapid slide of rock and earth and of flow of debris and earth [35]. After the 2010 activation, the landslide showed a subvertical main scarp of about 50 m (Figure 1B) and an overall length of about 1400 m; the main failure surface developed within the hemipelagic marls at a maximum depth of 50 m. During the landslide paroxysmal phase, a significant portion of the Calcare di Base Formation, close to the failure surface, collapsed so changing its mechanical characteristics and assuming a viscous fluid behavior (Figure 1B). This destructured and fluidized limestone allowed a rafting of large rocky blocks without severe disturbance [35].

On 20 February 2010, the main scarp of the Maierato landslide was affected by a retreat of about 80 m (Figure 1B) that affected a surface of about  $2 \times 10^4 \text{ m}^2$  and a volume of about  $4 \times 10^5 \text{ m}^3$ . The landslide, during the 2010 paroxysmal phase, was filmed by an cameraman of a private broadcast company, and is still available online (<https://www.youtube.com/watch?v=oWHjBsvmyLc>).

In this paper, by the use of landslide map, photo time series and, in particular, UAVs we were able to: (i) describe the geometry of the Maierato landslide; (ii) assess the morphological/topographical changes linked to the landslide evolution over the last ten years; (iii) exploit the SfM algorithm to salvage post event pictures and quantify landslide magnitude; (iv) assess the effectiveness of the UAV and the structure from motion approach in order to contribute to manage residual risk in the medium and long term within an integrated geotechnical monitoring network.

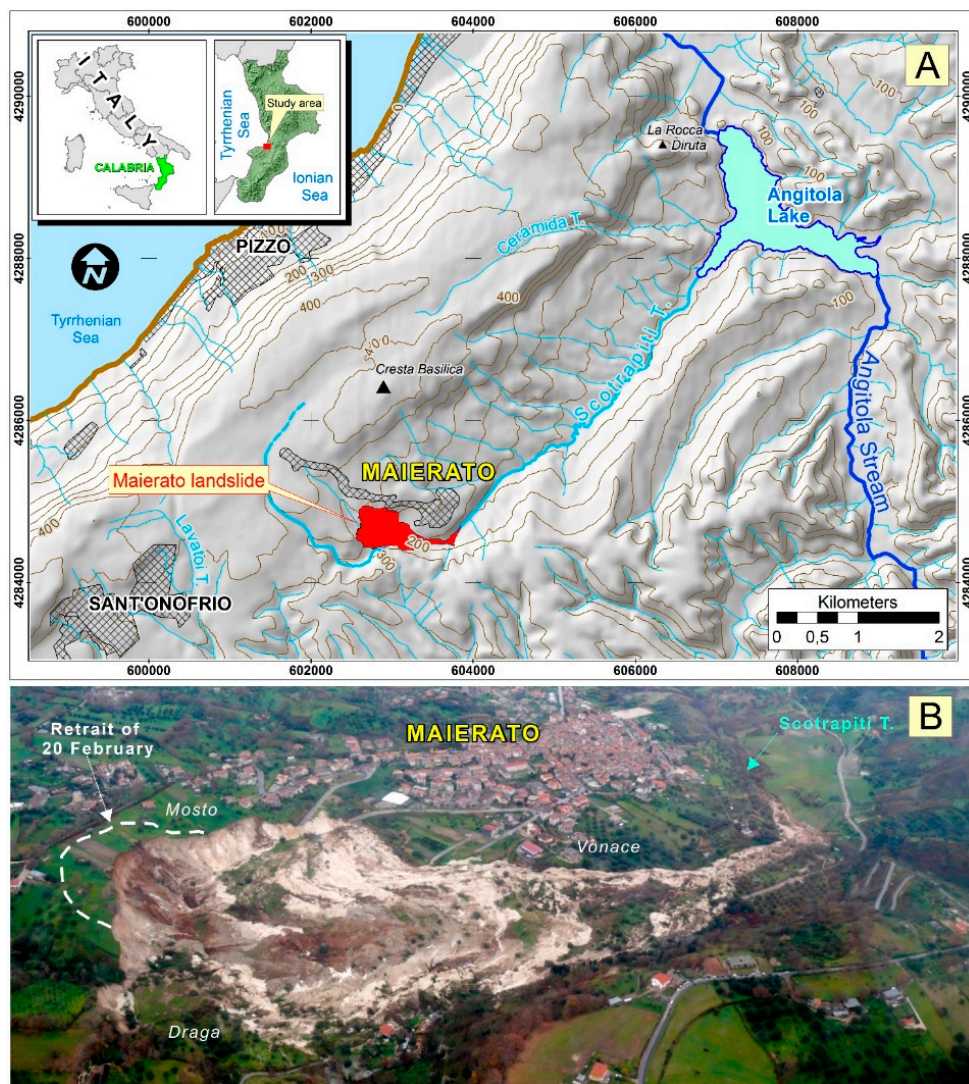


**Figure 1.** Location (A) and panoramic view (B) of Maierato landslide occurred on 15 February 2010 (helicopter photo taken on 16 February 2010, by G.G.).

## 2. Methods and Materials

The workflow of the proposed methodology is shown in Figure 2 and used as main tool a periodic monitoring by UAV [41]. The monitoring of the landslide was initiated after the event with a conventional approach [35,39], particularly the geomorphological study of the area (Figure 1B) was performed through analyses of Google Earth™ multi-temporal high-resolution satellite images and detailed multi-temporal field surveys performed between 2010 and 2019. The updated landslide inventory was mapped on a 1:5000 topographic base map and implemented in a geographic information system (GIS).

Type and state of activity of mapped landslides were attributed following the classification proposed by [42], and using geomorphological criteria based on field reconnaissance of gravity-related landforms, including scarps, conjugate scarps, irregular slope profiles, ground cracks, changes in the drainage network, and damages to infrastructures (Figures 3 and 4). Afterwards, the comparison of photos taken at different times (in the last 10 years) has allowed us to qualitatively evaluate, by visual inspection, the morphological variations in the area affected by the 2010 landslide (Figure 5).

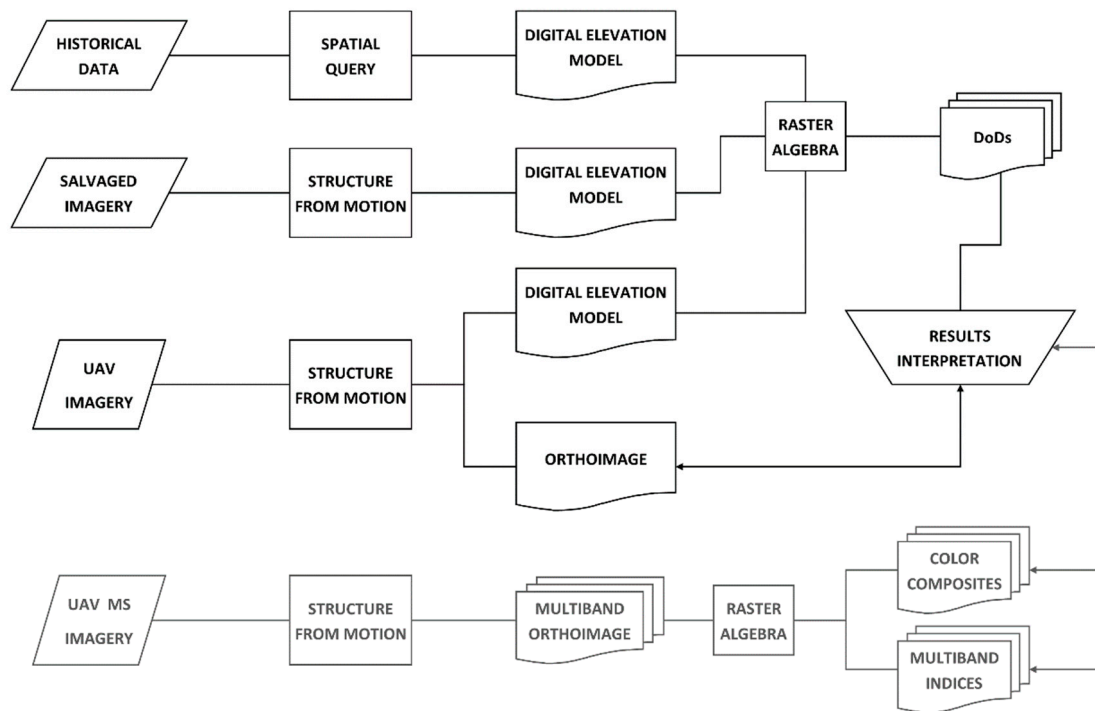


**Figure 2.** Workflow of the proposed methodology, the grey sector was only carried out with an experimental approach.

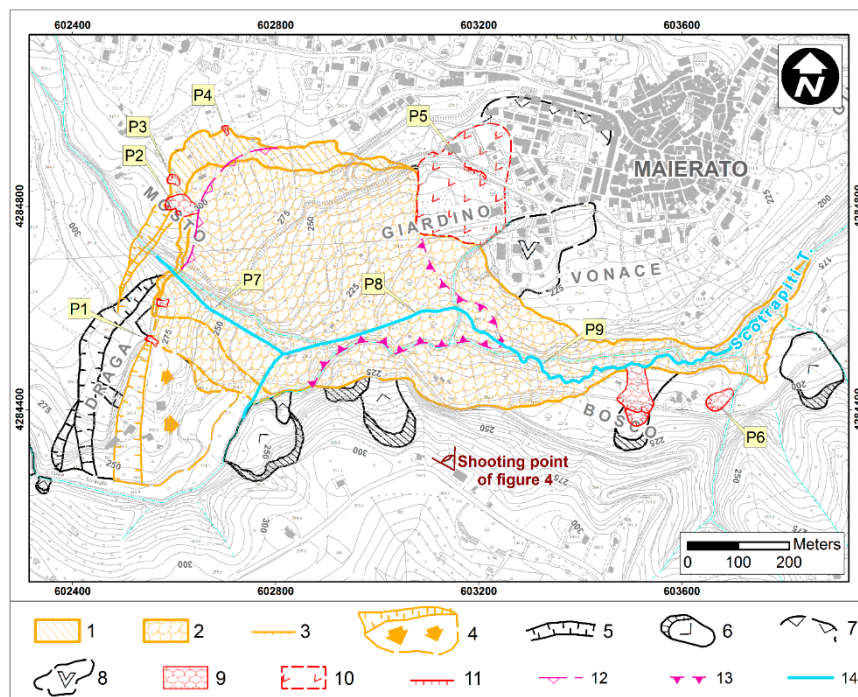


**Figure 3.** Landslide map and locations of the available photographs (shown in Figure 4). Legend: (1) 20 February 2010 landslide scarp; (2) 20 February 2010 landslide body; (3) 20 February 2010 secondary landslide scarp; (4) Draga active block-slide delimited by active graben-like trench; (5) dormant trench; (6) dormant slide; (7) ancient landslide scarp; (8) ancient block-slide with uncertain boundary; (9) 2018 landslide body; (10) active landslide body; (11) 2018 landslide scarp; (12) trace of 15 February 2010 main scarp; (13) toe of the 15 February 2010 sliding surface; (14) Scotrapiti Torrent (present course).



**Figure 4.** Photographs representing landslides (red arrows) activated in 2018 (P1–P6) and the current deepening action with local stream bank erosion along the Scotrapiti Torrent (P7–P9) (photo locations in Figure 3).

The monitoring was resumed recently in order to quantitatively assess the landslide evolution and its residual risk. The depicted geomatic approach entailed several steps. In the first one, in order to evaluate the differences between the pre and post event phases, a pre-failure Digital Terrain Model (DTM) was retrieved from the Maierato municipal administration; the DTM was interpolated from a 1:5000 scale topographic map surveyed in 1996. In the second step, thanks to the availability of a post event image set, taken from a helicopter-borne (Figure 1B), executed immediately after the landslide event (on 16 February 2010), an attempt to reconstruct the geometry of the landslide and its DTM in its aftermath was carried out by using computer vision approach. In the third step, the entire landslide area was surveyed (on December 2017 and November 2018) with a DJI Phantom 4 Pro™ with the purpose of obtaining digital elevation models and orthoimages. The two UAV photogrammetric (PG) flights were planned according to Table 1. Finally, to test the capability of multispectral sensor and to provide additional information in the interpretation of the landslide evolution [43] an additional UAV multispectral (MS) flight was carried out with the same quadcopter equipped with a Micasense RedEdge™ Sensor [44].

**Table 1.** Unmanned aerial vehicle (UAV) flights characteristics.

Date	Type	Sensor
05 Dember 2017	PG	1" CMOS (20 MPixel) Lens FOV 84° 8.8 mm/24 mm (35 mm format equivalent) f/2.8–f/11 auto focus
27 November 2018	PG	ISO Photo: 400 Shutter Speed: 1/1000 s Shutter mode: time priority
27 November 2018	MS	Micasense RedEdge (5 bands) 3.6 MPixel/band

During every flight, in order to allow their geocoding, several targets were deployed in the surveyed area and their coordinates determined by a GNSS, Leica 1200™ receiver, in VRS mode [45], assuring a centimetric accuracy. Each image set (UAV or salvaged) was then post processed with Agisoft Metashape™. In the software images were aligned and geocoded by surveyed target collimation. Finally thanks to the SfM algorithm [46–48] a 3D model was reconstructed. Additionally, for hypothetical visual interpretation purposes RGB orthoimages were computed, too.

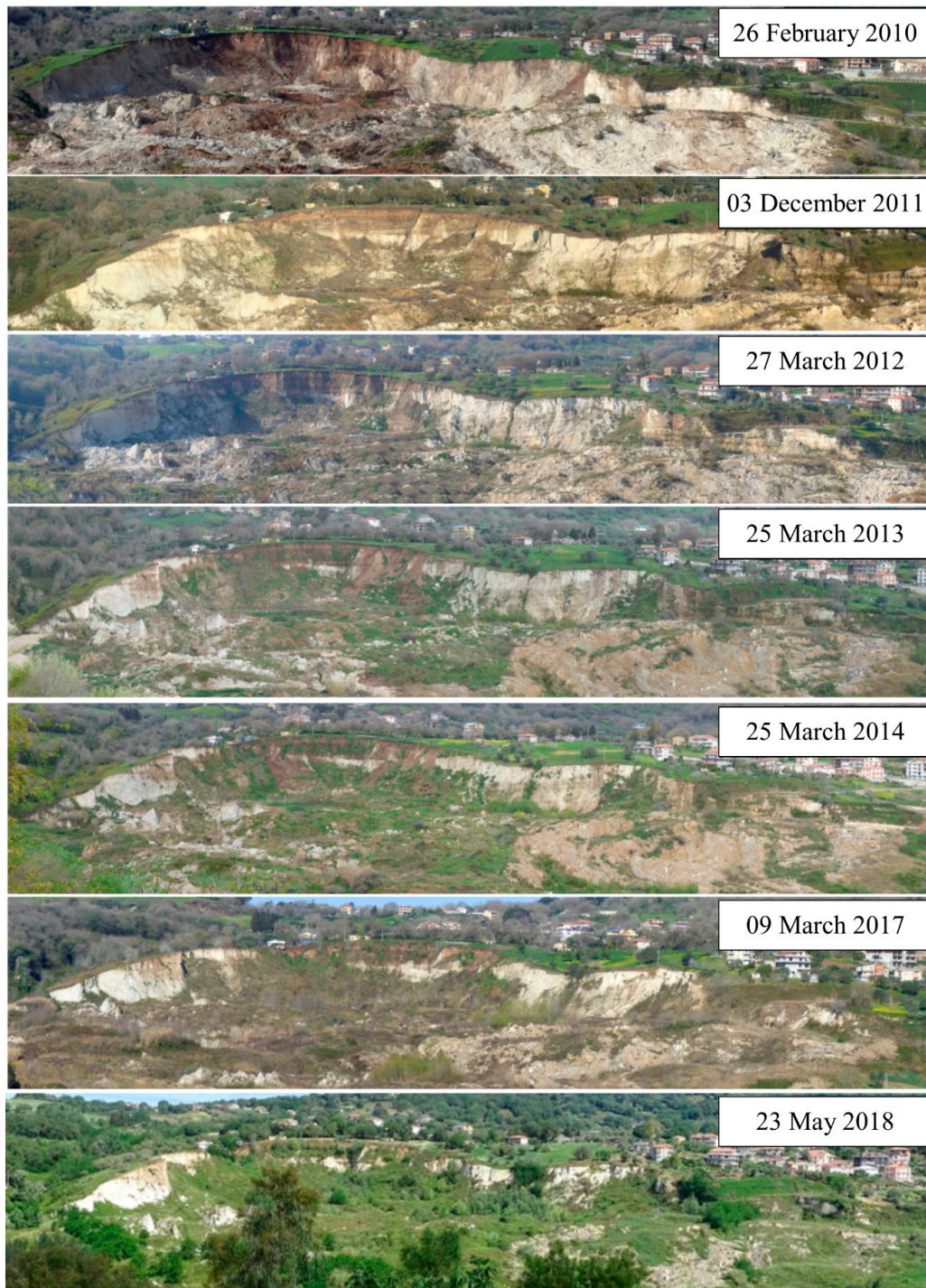


**Figure 5.** Panoramic images time series showing the evolution of the Maierato landslide scarp in the last years.

The salvaged images, 49 photos taken from a Panasonic DMC-FZ50, were processed through the same procedure adopted with PG and MS, too. The co-registration was performed by the collimation of feature recognizable in the November 2018 orthoimage and by entering the coordinates as extracted by the relative orthoimage and Digital Elevation Model (DEM). The processing allowed to compute a DEM and an orthoimage of the landslide area. Concerning the MS flight, the multiband dataset was processed in the same way obtaining a 3D model and a multiband orthoimage. The obtained raster layers (Table 2) were then processed in an open source GIS environment [49] where, through a raster algebra approach, several DEM of differences (DoD) were computed with the purpose of quantifying the morphological variation induced by the landslide in the last 10 years.

**Table 2.** DTM technical features.

Year	Source	Methodology	Ground Resolution [m]	Point Density [points/m <sup>2</sup> ]	Image Type
1996	Technical map	Interpolation	5.00	NA	NA
2010	Reconnaissance	SfM	0.60	2.85	RGB
2017	UAV	SfM	0.05	402	RGB
2018	UAV	SfM	0.05	419	RGB

### 3. Results

The monitoring actions provided information concerning the landslide evolution. They can be subdivided in two main categories as the conventional approach mainly supplied qualitative description of the landslide state, while the other one gave quantitative data describing the evolution of the monitored phenomenon.

#### 3.1. Conventional Monitoring

Multitemporal geomorphological field surveys, performed between 2010 and 2019 (whose results are summarized in Figure 3), showed that the Maierato landslide during this period of time has not undergone substantial modifications. Only minor and localized instability phenomena occurred along the main scarp and the margins of the landslide body during the last few years. Specifically, some debris slides of modest size affected the crown of the Maierato landslide (Figure 4, red arrows in photo P1–P4), linked to the attainment of the geostatic balance of the main scarp. Two phenomena typologically related to roto-translational active slides were detected in the Bosco area (Figure 4, photo P6), while a larger slide with an uncertain body, also in a state of activity, was detected in the Giardino area (Figure 4). This slow-moving landslide causes a lowering of the roadway point out by shear or tensile fractures (Figure 4, P5).

In the same period of time, the geomorphological field surveys also show, along the new course of the Scotrapiti Torrent, in the middle and low portion of the 2010 landslide body, a progressive deepening action of the river bed associated with local riverbank erosion phenomena (Figure 4, P7–P9).

The multitemporal comparison of panoramic photos (time span from 26 February 2010 to 23 May 2018) of the upper portion of the landslide phenomenon does not show any remarkable retreat of the main scarp and its crown (Figure 5), while it allows to observe a variation of the soil coverage mainly determined by the regrowth of vegetation (trees and shrubs) in the area affected by the landslide. Moreover, in the same time interval, the comparison of the photos shows a generalized lowering of the topographic surface in the landslide body mainly linked to the disintegration and compaction of the lithotypes involved in the mass movement (Figure 5).

#### 3.2. Geomatic Monitoring

Concerning UAV surveys, the SfM algorithm has proved its effectiveness by providing reliable results in processing surveyed imagery (RGB and multispectral). It has also allowed taking advantage

even of the salvaged dataset, acquired with completely different purposes (Figure 6) and, to compute an unprecedented DEM. The registration and co-registration procedures provided results as much accurate as the SfM performance as shown in Table 3.



**Figure 6.** Examples of reconnaissance photographs taken from helicopter (on February 16, 2010), characterized by obstacles in the frame (A) or very oblique shot (B).

**Table 3.** Registration/co-registration errors.

Year	GCP	XY Error [cm]	Z Error [cm]	Total Error [cm]
2010	8	63.09	14.29	64.69
2017	11	2.67	2.25	3.49
2018	13	1.12	0.54	1.24

By exploiting the pre-failure 1996 DTM, and the 16 February 2010 DTM, it was possible to quantify the variations occurred immediately after the landslide (Figure 7, DoD 1996–2010). The obtained DoD highlighted the formation of a scarp of up to 54 m and of a deposition area of comparable height. The DoD 2010–2017 highlights both the landslide scarp retrogression (which took place on 20 February 2010), which produces a lowering of the topographic surface of about 40 m, and emphasizes several evolution phenomena in the deposit sector of the landslide (Figure 7, DoD 2010–2017); it is, in fact, clearly evident the onset of an erosion process in the riverbed of Scotrapiti Torrent which was channeled through the landslide deposit. The DoD 2017–2018 highlights small topographical variations within the landslide affected area. In particular, the channel sector is characterized by the growth of poplar and willow trees, while the upper part of the deposit sector is characterized by erosion processes that bring to light large rock blocks (where the original stratigraphy is preserved), characterized by higher density, showing an initial onset of pioneer vegetation (Figure 7, DoD 2017–2018). Finally, the overall topographical/morphological changes of the landslide affected area are shown in the DoD 1996–2018 (Figure 7).

To provide additional information in the interpretation of the landslide evolution, the experimental MS flight was successfully carried out [49]. The UAV set-up with customized supports (Figure 8, inset), crafted with a 3D printer, allowed to perform the survey without remarkable influence on UAV flight stability and duration. The preliminary result, a Color-infrared (CIR) composite [50] orthoimage (Figure 8), provided an identification of some sectors characterized by dense tree cover in clear stress (Figure 8A–C) or by several trees in healthy condition (Figure 8D). These results offer the opportunity for additional insights into the interpretation of the current state of the landslide deposit.

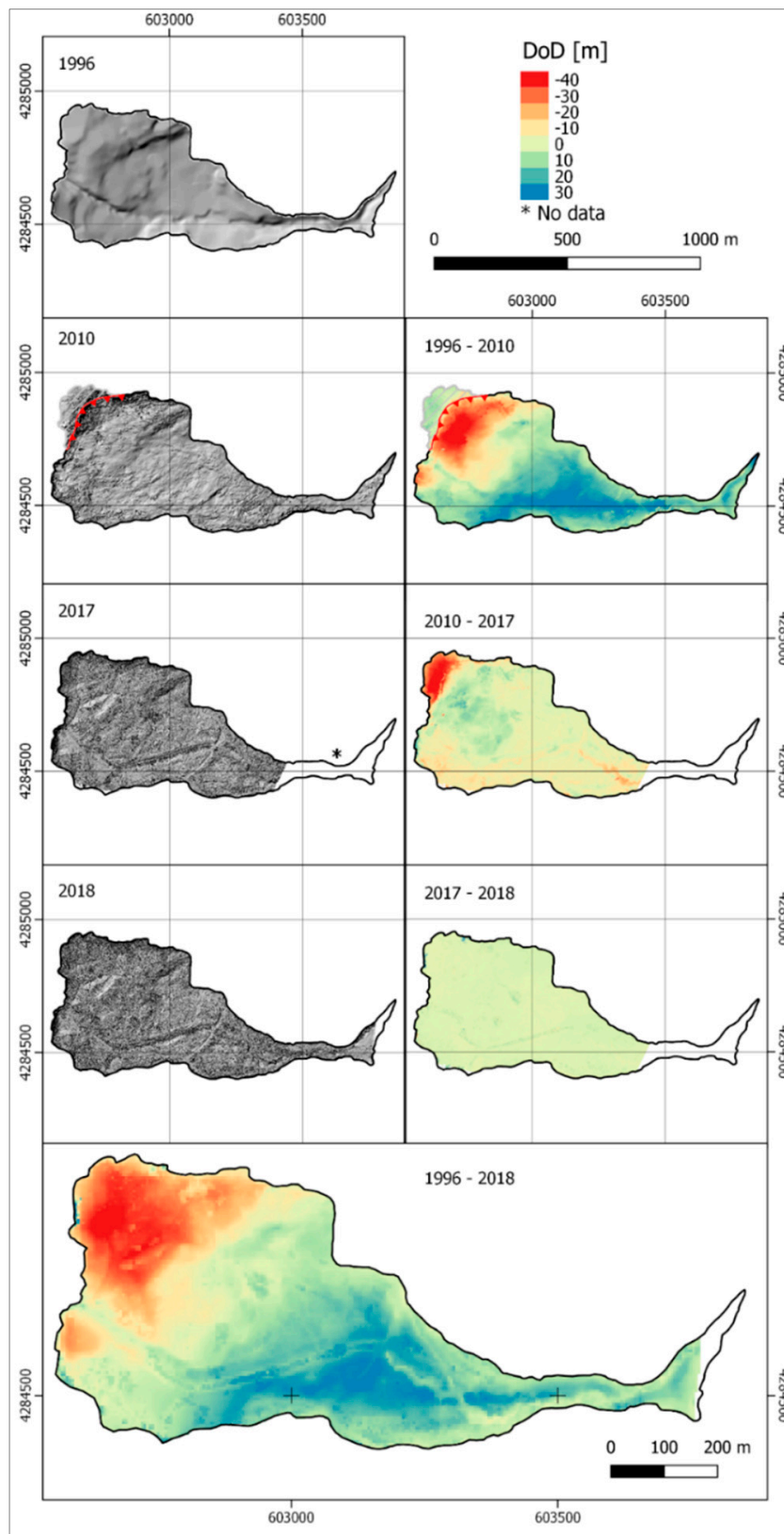


**Figure 7.** Hillshades (left) and DEM of differences (DoDs) (right) of the landslide (RS: UTM WGS84—Zone 33N; EPSG code 32633). The red line in the 2010 hillshade and in the 1996–2010 DoD represent the landslide scarp of 15 February 2010.

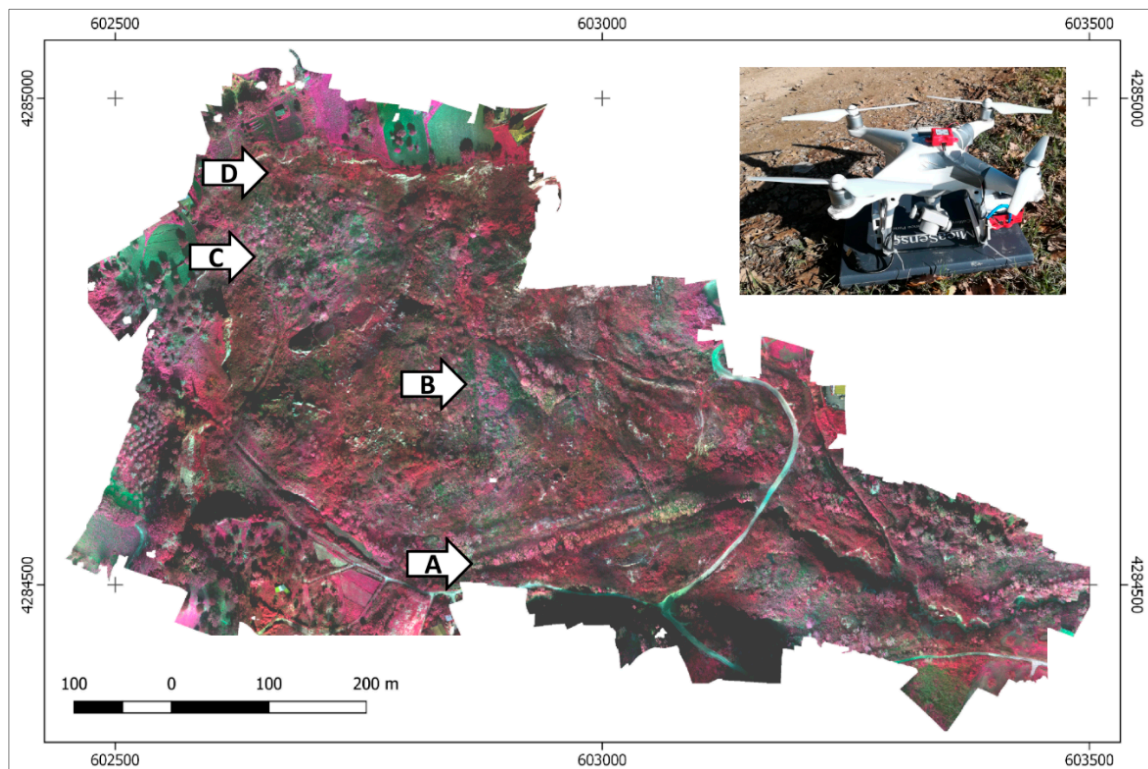


**Figure 8.** CIR orthoimage resulted from the multispectral (MS) flight; in the inset picture: UAV equipped with MS sensor. Arrows indicates peculiar sectors of the orthoimage where vegetation dynamics are interpreted.

#### 4. Discussion

The presented results and methodology (Figure 9) showed that the repeated geomorphological surveys (Figure 3) constitute the basis for the next monitoring operations, including UAV flights. The surveys, indeed, highlighted, besides those pointed out by the geomatic monitoring, the absence of remarkable evolutionary phenomena during the investigated time span. Additionally, the helicopter borne reconnaissance photos (February 2010) have provided supplementary data for the processing and the subsequent analyses. In fact, the capabilities of the SfM algorithm have allowed to exploit the availability of images taken immediately after the landslide occurrence and to compute unprecedented 3D data of landslide aftermath. In particular, the availability of previous 3D public dataset allowed to quantify the evolution of the landslide deposit and morphological features, i.e., scarp evolution (Figure 7, DoD 1996–2010). With respect to the aftermath surveys [39,46] the results obtained from the proposed methodology allowed to quantify variations from the original topography ranging from  $-54.8$  m, in the main scarp sector, to  $37.1$  m in the deposit sector. Moreover, the mobile targets combined with the GNSS-VRS allow to register the images in a quick mode optimizing the positioning phase, with the aim of co-registering the survey time series in a repeatable way. Additionally, the adopted method avoids fixed targets installation thus reducing field work and the risk of target damaging. On the other hand, UAV survey is heavily affected by tree canopy cover that can mask ground portion [51,52] thus preventing their measurements, the final 3D model will, in fact, represent, in these areas, the canopy surface instead of the terrain. Concerning the comparison between the first UAV survey (2017) and the 2010 3D model (Figure 7, DoD 2010–2017), the remarkable topographic changes, occurred between 15th and 20th February 2010, are pointed out. In the scarp sector an additional collapse caused a retreat of the crown of up to  $96.7$  m and an elevation reduction of  $54.0$  m. On the other hand, in the central sector a residual deposition of  $18.7$  m occurred. In the southern landslide border an elevation reduction,

ranging from 1.7 to 9.9 m, is observable. Moreover, the onset of the erosion of the non-channeled segment of the Scotrapiti Torrent is distinctly represented.

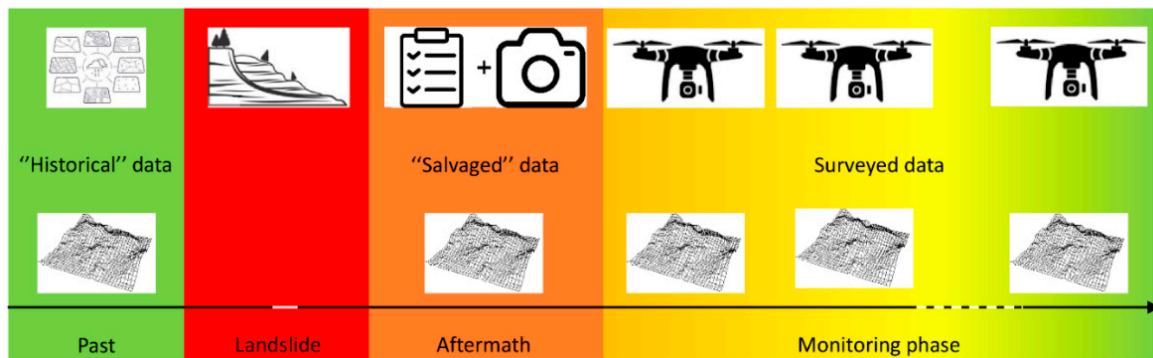


Figure 9. Recapitulatory scheme of the proposed methodology.

The evaluation of the differences between the two UAV 3D models (Figure 7, DoD 2017–2018) at a homogeneous scale color reveals non-substantial changes. However, an additional representation with a customized color scale (Figure 10) has provided insights of the local variations of the investigated areas. Particularly the progress of the erosive processes in the lower stretch of the Scotrapiti Torrent is visible. A diffuse, yet shallow, erosive dynamic can be noticed in the main scarp sector, too. The areas still featuring an elevation increase show the growth of vegetation in the channeled part of the Scotrapiti Torrent and in other sector of the deposit.

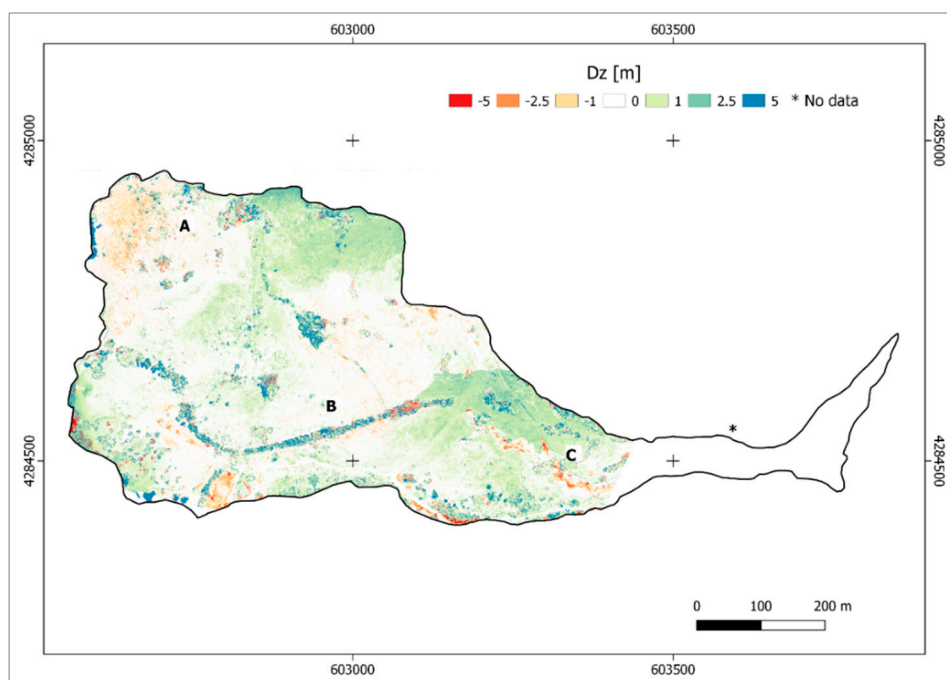


Figure 10. Detail of the 2017–2018 DoD with a customized color scale.

Generally, the UAV survey allowed to quantify the modification occurred from the event until the last flight. In the DoD 1996–2018 of Figure 7, the elevation reduction in the crown sector reached values up to  $-46.7$  m, conversely in the deposit sector the maximum increase in elevation resulted as  $35.5$  m.

Concerning DTM accuracies and resolutions the three datasets (pre-failure, salvaged and UAV) are characterized by different orders of magnitude. The heterogeneous spatial resolution and registration errors of the analyzed 3D models could constitute an issue for the correct evaluation of landslide

modifications. However, concerning the pre failure DTM, it was the only available one and the scale and resolution are comparable or better than similar dataset used in regional cartographic datasets in Italy [53,54]. UAV DEMs are the best products, among the analyzed dataset, and are, currently, the state of the art of airborne mapping. The salvaged dataset is the critical one because of its uniqueness. Without it, the computation of the aftermath modifications would not be feasible and the whole reconstruction would have been incomplete. The computation of DoD 1996–2010 compared analogous datasets in terms of resolution and accuracy. Conversely, the following one (i.e., DoD 2010–2017) evaluated differences between two DEM characterized by remarkably different features. As mentioned above, the salvaged dataset was exploited thank to the SfM capabilities and without them it would have been remained a series of pictures taken from the helicopter to document the landslide aftermath without any metric attribute. Moreover, the magnitude of the investigated phenomenon is, by far, greater than the characteristic of the worst DEM used. The same matter concerns the 1996–2018 DoD where the comparison is computed between 2018 and 1996 DEMs and equally the scale of the computed differences exceeds the rasters resolution and accuracy issues. Lastly, concerning 2017–2018 DoD the two DEM are comparable both in resolution and accuracy.

Definitely, the UAV surveys resulted in an effective spatial representation of the studied area, allowing a continuous analysis of the investigated phenomenon. The repeated survey highlighted, contemporarily, several evolutionary processes dynamics in different landslide sectors (Figure 11), mainly in the scarp and in the main body: (i) retrogressive evolution of the scarp; (ii) erosion of the main body; (iii) onset of pioneer vegetation; (iv) erosion in the non-channeled riverbed of the Scotrapiti.

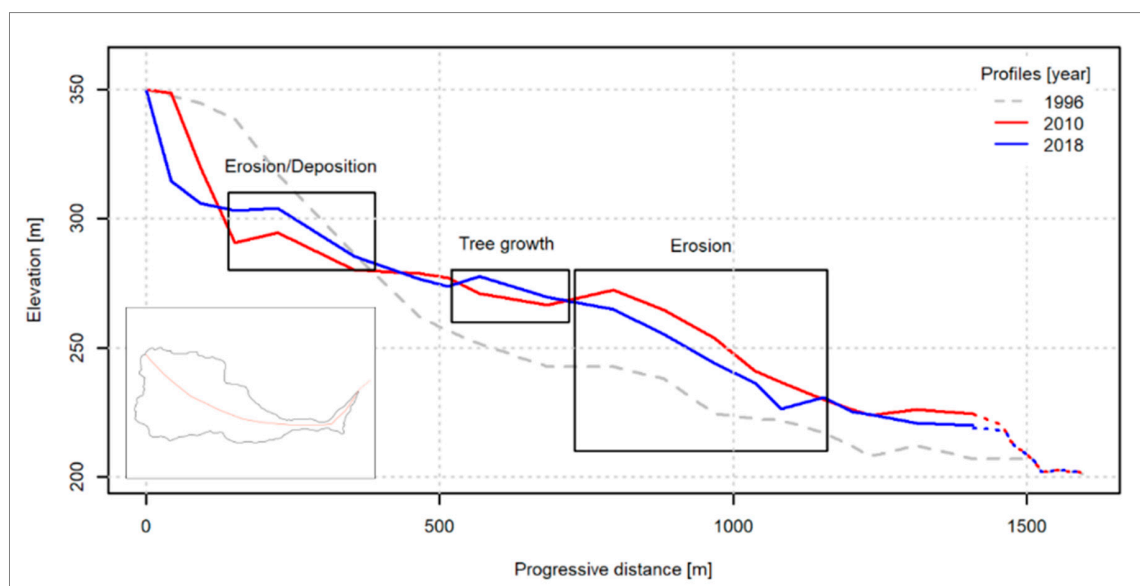


**Figure 11.** Cross section comparison depicting landslide evolution, the dotted lines represents the hypothetical profile outside the landslide border connecting with the undisturbed one.

Concerning residual risk assessment, the retrogressive dynamic, that represent the most critical phenomenon, as it can endanger area previously unaffected by the landslide, is also confirmed by qualitative comparison of homologous features recognizable in the reconnaissance image set and in the UAV imagery (e.g., Figure 12 clearly show the scarp evolution in correspondence of a manure-heap located in the crown area). Moreover, Figure 12C shows the pre- and post-landslide position of a building located in the landslide area and the displacement of 98.4 m measured from the comparison between 2010 and 1996 DTMs, confirmed by the same analysis carried out on 2018 and 1996 DTMs which did not highlight further shift.



**Figure 12.** Evaluation of retrogressive evolution of the landslide: qualitative comparison between the terrestrial reconnaissance photograph (A) and the UAV survey (B); (C) measurement of the displacement of a building moved by the landslide.

The experimental MS survey provided additional hints for the interpretation of the phenomena in the post emergency phase. Particularly (Figure 13), sector A identifies a stretch of Scotrapiti Torrent featuring a dense tree cover in clear stress [55]; the same condition is present in sectors B and C where pioneer vegetation struggle to colonize landslide displaced materials characterized by scarcely evolved soils. On the other hand, in some sectors close to the landslide crown (sector D) there are several trees in healthy condition, due to the translation of large mixed blocks, preserving the integrity of roots and topsoil. The execution of a second flight could add further elements and allow the accomplishment of a change detection analysis for an in deep investigation.

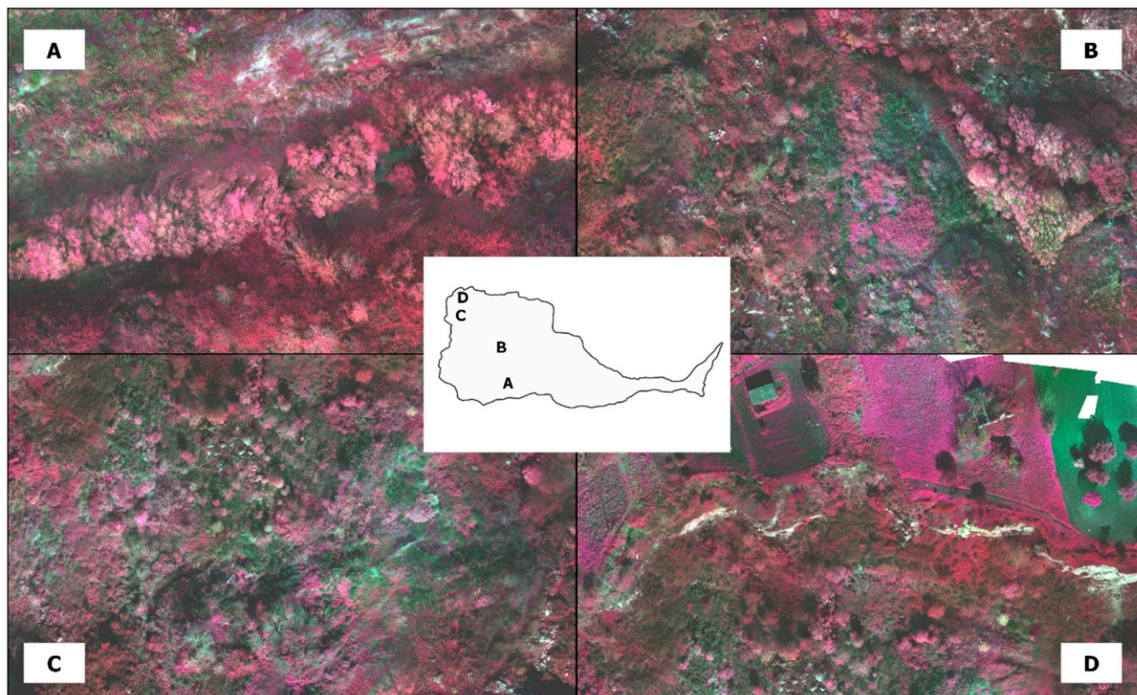


**Figure 13.** Details of four peculiar sectors of the landslide depicting different vegetation behavior that could be related with local dynamics.

## 5. Conclusions

The peculiar kinematic features of the Maierato landslide make long-term monitoring of the surrounding area necessary, in order to identify any instability directly connected to the 2010 landslide and, although unlikely, the occurrence of morphological and/or kinematic “indicators” that highlight the possible activation of instability conditions similar to those that led to the 2010 landslide. In the area of interest, an integrated monitoring was carried out immediately after the landslide activation, which allowed the management of the residual risk in the immediacy of the event (emergency phase), in the post-emergency one and for a significant period in ordinary conditions.

The remarkable photographic documentation acquired in the immediate post-event phase, from helicopter and ground surface, provided useful qualitative indications in the analysis of the results of the conventional integrated monitoring. Additionally, in the subsequent ordinary phase, the multi-temporal geomorphological surveys were carried out to qualitatively monitor the post emergency evolution of the landslide and to assess future actions.

The need to obtain monitoring data for long term management of residual risk suggested the opportunity to experiment UAV surveys and image processing algorithms (i.e., SfM), in order to acquire quantitative and more detailed data concerning geometrical/morphological changes between the condition prior to the 2010 landslide, immediately after the landslide event and several years after its occurrence. The obtained results indicate that the store of knowledge improve the experimental processing of the post event photographs and the comparison with previous data. Indeed, the analyses carried out have allowed to better comprehend the post event evolution of the Maierato landslide and to confirm the capabilities of UAV and SfM in landslide monitoring. The methodologies have provided promising results, as their features (accuracy, resolution, etc.) are compatible with the magnitude of the investigated event, and insights which have confirmed the validity of the approach and the possibility of the integration with conventional ones, in order to better monitor and comprehend the studied phenomenon’s dynamics and evolution in the medium-long period. Definitely, the proposed UAV monitoring (Figure 9) confirmed its validity by assuring a cost-effective methodology, as it reduces

survey time (i.e., every campaign is executable in one day) and, contemporarily, ensures the quality of the final results.

**Supplementary Materials:** The supplementary materials are available online at <http://www.mdpi.com/2072-4292/12/6/1039/s1>.

**Author Contributions:** Conceptualization, P.A., L.B. and G.G.; data curation, D.G. and P.A.; formal analysis, P.A., L.B. and G.G.; investigation, D.G.; methodology, D.G., P.A., L.B. and G.G.; project administration, G.G.; resources, G.G.; software, D.G. and P.A.; supervision, P.A. and G.G.; validation, D.G. and P.A.; visualization, D.G. and L.B.; writing—original draft, D.G.; writing—review and editing, P.A., L.B. and G.G. All authors have read and agreed to the published version of the manuscript.

**Funding:** This research was partially funded by “Accordo per Supporto tecnico-scientifico per il monitoraggio delle frane, la pianificazione e la valutazione degli interventi di mitigazione del rischio da frana nell’area urbana di Maierato”, CNR-IRPI – Comune di Maierato (VV)”.

**Acknowledgments:** The authors kindly acknowledge Enzo Valente, Salvatore Guardia and Luigi Aceto for the technical support provided.

**Conflicts of Interest:** The authors declare no conflict of interest.

## References

- Gariano, S.L.; Guzzetti, F. Landslides in a changing climate. *Earth Sci. Rev.* **2016**, *162*, 227–252. [[CrossRef](#)]
- Soldati, M.; Corsini, A.; Pasuto, A. Landslides and climate change in the Italian Dolomites since the Late glacial. *Catena* **2004**, *55*, 141–161. [[CrossRef](#)]
- Kirschbaum, D.B.; Adler, R.; Hong, Y.; Hill, S.; Lerner-Lam, A. A global landslide catalog for hazard applications: Method, results, and limitations. *Nat. Hazards* **2010**, *52*, 561–575. [[CrossRef](#)]
- Gullà, G.; Caloiero, T.; Coscarelli, R.; Petrucci, O. A proposal for a methodological approach to the characterisation of widespread landslide events: An application to Southern Italy. *Nat. Hazards Earth Syst. Sci.* **2012**, *12*, 165–173. [[CrossRef](#)]
- Aleotti, P.; Chowdhury, R. Landslide hazard assessment: Summary review and new perspectives. *Bull. Eng. Geol. Environ.* **1999**, *58*, 21–44. [[CrossRef](#)]
- Borrelli, L.; Gullà, G. Tectonic constraints on a deep-seated rock slide in weathered crystalline rocks. *Geomorphology* **2017**, *290*, 288–316. [[CrossRef](#)]
- Aceto, L.; Antronico, L.; Borrelli, L.; Coscarelli, R.; Pasqua, A.A.; Petrucci, O.; Reali, C.; Guardia, S.; Valente, E. Relazione Attività Svolte—Comune di Maierato. “Studi ed Indagini Geologiche, Geotecniche, Idrologiche ed Idrauliche nel Comune di Maierato” “Monitoraggio Finalizzato alla Gestione Dell’emergenza nel Comune di Maierato” “Studi ed Indagini Geologiche, Geo. 2014. Available online: <http://www.cnr.it/prodotto/i/288410> (accessed on 3 December 2019).
- Gullà, G.; Aceto, L.; Antronico, L.; Borrelli, L.; Coscarelli, R.; Perri, F. A smart geotechnical model in emergency conditions: A case study of a medium-deep landslide in Southern Italy. *Eng. Geol.* **2018**, *234*, 138–152. [[CrossRef](#)]
- Gullà, G.; Calcaterra, S.; Gambino, P.; Borrelli, L.; Muto, F. Long-term measurements using an integrated monitoring network to identify homogeneous landslide sectors in a complex geo-environmental context (Lago, Calabria, Italy). *Landslides* **2018**, *15*, 1503–1521. [[CrossRef](#)]
- Gullà, G.; Peduto, D.; Borrelli, L.; Antronico, L.; Fornaro, G. Geometric and kinematic characterization of landslides affecting urban areas: The Lungro case study (Calabria, Southern Italy). *Landslides* **2017**, *14*, 171–188. [[CrossRef](#)]
- Chae, B.G.; Park, H.J.; Catani, F.; Simoni, A.; Berti, M. Landslide prediction, monitoring and early warning: A concise review of state-of-the-art. *Geosci. J.* **2017**, *21*, 1033–1070. [[CrossRef](#)]
- Mikkelsen, P.E. Field instrumentation. *Spec. Rep. Natl. Res. Counc. Transp. Res. Board* **1996**, *247*, 278–316.
- Krauter, E. Special lecture: Applicability and usefulness of field measurements on unstable slopes. In Proceedings of the International Symposium on Landslides. 5, Lausanne, Switzerland, 10–15 July 1988; Volume 1, pp. 367–373.

14. Arbanas, Ž.; Sassa, K.; Nagai, O.; Jagodnik, V.; Vivoda, M.; Jovančević, S.D.; Peranić, J.; Ljutić, K. A landslide monitoring and early warning system using integration of GPS, TPS and conventional geotechnical monitoring methods. In *Landslide Science for a Safer Geoenvironment: Volume 2: Methods of Landslide Studies*; Springer International Publishing: Cham, Switzerland, 2014; pp. 631–636. ISBN 9783319050508.
15. Calcaterra, S.; Cesi, C.; Di Maio, C.; Gambino, P.; Merli, K.; Vallario, M.; Vassallo, R. Surface displacements of two landslides evaluated by GPS and inclinometer systems: A case study in Southern Apennines, Italy. *Nat. Hazards* **2012**, *61*, 257–266. [[CrossRef](#)]
16. Hong, C.Y.; Zhang, Y.F.; Li, G.W.; Zhang, M.X.; Liu, Z.X. Recent progress of using Brillouin distributed fiber optic sensors for geotechnical health monitoring. *Sens. Actuators A Phys.* **2017**, *258*, 131–145. [[CrossRef](#)]
17. Lollino, G.; Arattano, M.; Cuccureddu, M. The use of the automatic inclinometric system for landslide early warning: The case of Cabella Ligure (North-Western Italy). *Phys. Chem. Earth Parts A B C* **2002**, *27*, 1545–1550. [[CrossRef](#)]
18. Allasia, P.; Lollino, G.; Godone, D.; Giordan, D. Deep displacements measured with a robotized inclinometer system. In Proceedings of the 10th International Symposium on Field Measurements in Geomechanics—FMGM2018, Rio De Janeiro, Brazil, 16–20 July 2018.
19. Gullà, G. Field Monitoring in Sample Sites: Hydrological Response of Slopes with Reference to Widespread Landslide Events. *Procedia Earth Planet. Sci.* **2014**, *9*, 44–53. [[CrossRef](#)]
20. Jaboyedoff, M.; Ornstein, P.; Rouiller, J.-D. Design of a geodetic database and associated tools for monitoring rock-slope movements: The example of the top of Randa rockfall scar. *Nat. Hazards Earth Syst. Sci.* **2004**, *4*, 187–196. [[CrossRef](#)]
21. Gili, J.A.; Corominas, J.; Rius, J. Using Global Positioning System techniques in landslide monitoring. *Eng. Geol.* **2000**, *55*, 167–192. [[CrossRef](#)]
22. Baldo, M.; Bicocchi, C.; Chiocchini, U.; Giordan, D.; Lollino, G. LIDAR monitoring of mass wasting processes: The Radicofani landslide, Province of Siena, Central Italy. *Geomorphology* **2009**, *105*, 193–201. [[CrossRef](#)]
23. Tarchi, D.; Casagli, N.; Fanti, R.; Leva, D.D.; Luzi, G.; Pasuto, A.; Pieraccini, M.; Silvano, S. Landslide monitoring by using ground-based SAR interferometry: An example of application to the Tessina landslide in Italy. *Eng. Geol.* **2003**, *68*, 15–30. [[CrossRef](#)]
24. Torrero, L.; Seoli, L.; Molino, A.; Giordan, D.; Manconi, A.; Allasia, P.; Baldo, M. The use of micro-uav to monitor active landslide scenarios. In *Engineering Geology for Society and Territory—Volume 5: Urban Geology, Sustainable Planning and Landscape Exploitation*; Springer International Publishing: Cham, Switzerland, 2015; pp. 701–704. ISBN 9783319090481.
25. Stumpf, A.; Malet, J.P.; Allemand, P.; Pierrot-Deseilligny, M.; Skupinski, G. Ground-based multi-view photogrammetry for the monitoring of landslide deformation and erosion. *Geomorphology* **2015**, *231*, 130–145. [[CrossRef](#)]
26. Nichol, J.; Wong, M.S. Satellite remote sensing for detailed landslide inventories using change detection and image fusion. *Int. J. Remote Sens.* **2005**, *26*, 1913–1926. [[CrossRef](#)]
27. Tralli, D.M.; Blom, R.G.; Zlotnicki, V.; Donnellan, A.; Evans, D.L. Satellite remote sensing of earthquake, volcano, flood, landslide and coastal inundation hazards. *ISPRS J. Photogramm. Remote Sens.* **2005**, *59*, 185–198. [[CrossRef](#)]
28. Giordan, D.; Adams, M.S.; Aicardi, I.; Alicandro, M.; Allasia, P.; Baldo, M.; De Berardinis, P.; Dominici, D.; Godone, D.; Hobbs, P.; et al. The use of Unmanned Aerial Vehicles (UAV) for engineering geology applications. *Bull. Eng. Geol. Environ.* **2020**, in press.
29. Chao, H.; Cao, Y.; Chen, Y. Autopilots for small unmanned aerial vehicles: A survey. *Int. J. Control. Autom. Syst.* **2010**, *8*, 36–44. [[CrossRef](#)]
30. Westoby, M.J.; Brasington, J.; Glasser, N.F.; Hambrey, M.J.; Reynolds, J.M. “Structure-from-Motion” photogrammetry: A low-cost, effective tool for geoscience applications. *Geomorphology* **2012**, *179*, 300–314. [[CrossRef](#)]
31. Chudý, F.; Slámová, M.; Tomaščík, J.; Prokešová, R.; Mokroš, M. Identification of micro-scale landforms of landslides using precise digital elevation models. *Geosciences* **2019**, *9*, 117. [[CrossRef](#)]
32. Kaiser, A.; Neugirg, F.; Rock, G.; Müller, C.; Haas, F.; Ries, J.; Schmidt, J. Small-scale surface reconstruction and volume calculation of soil erosion in complex moroccan Gully morphology using structure from motion. *Remote Sens.* **2014**, *6*, 7050–7080. [[CrossRef](#)]

33. Marek, L.; Miřijovský, J.; Tuček, P. Monitoring of the shallow landslide using UAV photogrammetry and geodetic measurements. In *Engineering Geology for Society and Territory—Volume 2: Landslide Processes*; Springer International Publishing: Cham, Switzerland, 2015; pp. 113–116. ISBN 9783319090573.
34. Pajares, G. Overview and Current Status of Remote Sensing Applications Based on Unmanned Aerial Vehicles (UAVs). *Photogramm. Eng. Remote Sens.* **2015**, *81*, 281–330. [[CrossRef](#)]
35. Borrelli, L.; Antronico, L.; Gullà, G.; Sorriso-Valvo, G.M. Geology, geomorphology and dynamics of the 15 February 2010 Maierato landslide (Calabria, Italy). *Geomorphology* **2014**, *208*, 50–73. [[CrossRef](#)]
36. Nico, G.; Borrelli, L.; Di Pasquale, A.; Antronico, L.; Gullà, G. Monitoring of an Ancient Landslide Phenomenon by GBSAR Technique in the Maierato Town (Calabria, Italy). In *Engineering Geology for Society and Territory—Volume 2*; Springer International Publishing: Cham, Switzerland, 2015; pp. 129–133.
37. Gattinoni, P.; Scesi, L. Landslide hydrogeological susceptibility of Maierato (Vibo Valentia, Southern Italy). *Nat. Hazards* **2013**, *66*, 629–648. [[CrossRef](#)]
38. Guerricchio, A.; Doglioni, A.; Fortunato, G.; Galeandro, A.; Guglielmo, E.; Versace, P.; Simeone, V. Landslide hazard connected to deep seated gravitational slope deformations and prolonged rainfall: Maierato landslide case history. *Soc. Geol. Ital.* **2012**, *21*, 574–576.
39. Antronico, L.; Borrelli, L.; Gullà, G.; Sorriso-Valvo, M. La frana di Maierato (Calabria, Italia meridionale) del febbraio 2010: Caratteristiche geomorfologiche ed evoluzione. *GEAM Geogr. Ambient. Min.* **2010**, *2*, 15–26.
40. Conte, E.; Donato, A.; Pugliese, L.; Troncone, A. Kinematics of the Maierato Landslide (Calabria, Southern Italy). *Procedia Eng.* **2016**, *158*, 194–199. [[CrossRef](#)]
41. Cignetti, M.; Godone, D.; Wrzesniak, A.; Giordan, D. Structure from motion multisource application for landslide characterization and monitoring: The champlas du col case study, Sestriere, north-western Italy. *Sensors* **2019**, *19*, 2364. [[CrossRef](#)]
42. Cruden, D.; Varnes, D. Landslides: Investigation and mitigation. Chapter 3—Landslide types and processes. *Transp. Res. Board Spec. Rep.* **1996**, *247*, 36–75.
43. Allasia, P.; Baldo, M.; Giordan, D.; Godone, D.; Wrzesniak, A.; Lollino, G. Near Real Time Monitoring Systems and Periodic Surveys Using a Multi Sensors UAV: The Case of Ponzano Landslide. In *IAEG/AEG Annual Meeting Proceedings, San Francisco, California, 2018—Volume 1*; Springer International Publishing: Cham, Switzerland, 2018; pp. 303–310.
44. MicaSense Rededge 2019. Available online: <https://www.micasense.com/> (accessed on 4 November 2019).
45. Euler, H.J.; Keenan, C.R.; Zebhauser, B.E.; Wübbena, G. Study of a Simplified Approach in Utilizing Information from Permanent Reference Station Arrays. In Proceedings of the National Technical Meeting of the Satellite Division of the Institute of Navigation, (ION GPS 2001), Salt Lake City, UT, USA, 11–14 September 2001; Volume 104, pp. 371–391.
46. Lucieer, A.; Jong, S.M.D.; Turner, D. Mapping landslide displacements using Structure from Motion (SfM) and image correlation of multi-temporal UAV photography. *Prog. Phys. Geogr.* **2014**, *38*, 97–116. [[CrossRef](#)]
47. Turner, D.; Lucieer, A.; Watson, C.; Turner, D.; Lucieer, A.; Watson, C. An Automated Technique for Generating Georectified Mosaics from Ultra-High Resolution Unmanned Aerial Vehicle (UAV) Imagery, Based on Structure from Motion (SfM) Point Clouds. *Remote Sens.* **2012**, *4*, 1392–1410. [[CrossRef](#)]
48. Giordan, D.; Hayakawa, Y.; Nex, F.; Remondino, F.; Tarolli, P. Review article: The use of remotely piloted aircraft systems (RPASs) for natural hazards monitoring and management. *Nat. Hazards Earth Syst. Sci.* **2018**, *18*, 1079–1096. [[CrossRef](#)]
49. Cheng, Y.; Yu, T.; Egozi, R.; Tarolli, P. Pioneer Vegetation Detection by Hyperspectral Images on Temporal Landslides: A case study of Tzengwen catchment upstream, Taiwan. In Proceedings of the 19th EGU General Assembly, EGU2017, Vienna, Austria, 23–28 April 2017.
50. Dingle Robertson, L.; King, D.J.; Davies, C. Assessing Land Cover Change and Anthropogenic Disturbance in Wetlands Using Vegetation Fractions Derived from Landsat 5 TM Imagery (1984–2010). *Wetlands* **2015**, *35*, 1077–1091. [[CrossRef](#)]
51. Hodgson, M.E.; Jensen, J.; Raber, G.; Tullis, J.; Davis, B.A.; Thompson, G.; Schuckman, K. An Evaluation of Lidar-derived Elevation and Terrain Slope in Leaf-off Conditions. *Photogramm. Eng. Remote Sens.* **2005**, *71*, 817–823. [[CrossRef](#)]
52. Godone, D.; Giordan, D.; Baldo, M. Rapid mapping application of vegetated terraces based on high resolution airborne LiDAR. *Geomat. Nat. Hazards Risk* **2018**, *9*, 970–985. [[CrossRef](#)]

53. Conforti, M.; Pascale, S.; Robustelli, G.; Sdao, F. Evaluation of prediction capability of the artificial neural networks for mapping landslide susceptibility in the Turbolo River catchment (northern Calabria, Italy). *Catena* **2014**, *113*, 236–250. [[CrossRef](#)]
54. Taramelli, A.; Paola, R.; Ardizzone, F. Comparison of SRTM elevation data with cartographically derived DEMs in Italy LAMPRE View project Integrated assessment of geo-hydrological instability phenomena in the Apulia region, interpretative models and definition of rainfall thresholds for landsli. *Rev. Geogr. Acad.* **2008**, *2*, 41–52.
55. Pavanelli, D.; Gennari, A.; Sulpizi, L.; Cavazza, C. Vegetation Dynamics on Clay Landslides After Bioengineering Works: Three Case Studies in North Apennines, Italy. In *Recent Advances in Geo-Environmental Engineering, Geomechanics and Geotechnics, and Geohazards*; Springer: Cham, Switzerland, 2019; pp. 445–448.



© 2020 by the authors. Licensee MDPI, Basel, Switzerland. This article is an open access article distributed under the terms and conditions of the Creative Commons Attribution (CC BY) license (<http://creativecommons.org/licenses/by/4.0/>).